2026 IEEE International Conference on Robotics and Automation (ICRA 2026)
June 1-5, 2026. Vienna, Austria

Stair climbing for vehicles with articulated tracked arms: Closed-loop flippers control

Thales H. Silva[1] and Fernando Lizarralde[1]

Abstract— **Stair-climbing algorithms for tracked robots often neglect proper control of articulated arms, relying instead on a set of empirically predefined positions. In contrast, this work introduces a novel closed-loop control approach for mobile robots equipped with actively articulated tracked arms during stair climbing. The robot under consideration employs either wheels or tracks as its primary locomotion system, while the arms can be actuated to extend mobility when required. To perceive the environment, the robot is equipped with a depth sensor for stair detection and an IMU used exclusively for orientation estimation. The configuration of each lateral arm set is planned by modeling its differential kinematics as a planar kinematic chain subject to position constraints. Based on this model, a state-feedback control law is designed to guarantee stability and convergence, allowing the robot to climb stairs autonomously. The controller adapts the tracks to the stair geometry, enabling maneuvers that resemble a snake-like climbing motion. This improves traction, prevents abrupt movements, and avoids undesired floor collisions. The effectiveness of the proposed control scheme is demonstrated on a real robot, with experimental results validating its performance.**

I. Introduction

While assisting operators in complex scenarios, robots will inevitably encounter obstacles that enhance human mobility but prove challenging for themselves. In this group, a stairway, the most pragmatic way to link a set of surfaces in different levels, is one of the most common and troublesome obstacles for ground robots.

The ground robots can be categorized into three primary classes based on their locomotion systems [1]: legged, tracked, and wheeled. Legged robots are distinguished by their superior adaptability to uneven and unstructured environments, often surpassing the capabilities of wheeled and tracked platforms [2]. While tracked robots offer enhanced traction and better energy efficiency, they do so at the expense of maneuverability in complex terrains. In contrast, wheeled robots provide the highest energetic efficiency, though they possess lesser traction and the most limited adaptability to unstructured terrain.

To gather the best qualities of each locomotion system in one robot, hybrid configurations are adopted, combining legs, tracks, and wheels as in [3], [4], [5], [6]. Most of the literature on stair-climbing algorithms covers hybrid robots, with a primary locomotion system, such as large tracks or wheels, together with articulated tracked arms (in this context, usually referred to as flippers), used to enhance mobility and traverse obstacles. This group of robots, named Actively Articulated Tracked Robots (AATVs) [4], is robust, energy-efficient, relatively fast, and fit to travel long distances.

Although having great capabilities, the high number of DoF involved and the absence of a complete comprehension of the scenario make teleoperation very demanding for a human operator, especially while transposing obstacles, such as stairs.

For the AATV Rosi [3] in Figure 1 to climb stairs, the flippers should first be positioned so that the tracks can pull up the whole body. As the track advances, the contact between the arm and a step edge happens. A small advance on tracks or a change of arm position inevitably modifies the robot pose, which needs immediate correction. Such a task is complex and requires an experienced operator to control the robot, which justifies the design of a closed-loop control.

Despite the AATV's literature being vast and rich, it is a fact that none of the proposed works, except for [4], properly control the flippers or consider the transition between the staircase and the lower/upper floor. Usually, heuristic and empirical parameters are used for controlling flippers by just sending them to fixed positions based on discrete events.

A. Related work

Research on stair-climbing strategies for mobile robots has progressed from early sensor-based approaches to more sophisticated perception and control approaches. Early work by [7] implemented a stair-climbing algorithm on Urbie using accelerometers, sonar, and a monocular camera, though without effective sensor fusion. Later, [8] introduced an EKF-based fusion of gyroscopes and a camera, improving alignment and collision avoidance, while [9] enhanced perception by equipping the Silver robot with stereo cameras and laser scanners. Further contributions emphasized terrain modeling and trajectory control, such as the mapping strategy in [10] using multiple LIDARs and operator input, the kinematic planning framework in [4], and the structured-terrain perspective of [11], which optimized heading and traction but did not address continuous flipper control. Collectively, these works illustrate a shift from localized sensing to integrated perception and control, while challenges remain in achieving robust flipper management and reducing reliance on precise environment models.

B. Paper Contribution

In this work, a novel strategy for automatic management of flippers during stair climbing is proposed, relying on only two readily available variables: (1) robot orientation and (2)

[1] The authors are with the Dept. of Electric Eng., COPPE, Universidade Federal do Rio de Janeiro, Brazil. (thales.silva@coppe.ufrj.br)

This study was financed in part by the Coordenação de Aperfeiçoamento de Pessoal de Nível Superior - Brasil (CAPES) - Finance Code 001 and CNPq/Brazil.

Fig. 1: Hybrid AATV named ROSI developed for belt conveyor inspection. The main locomotion system is wheeled, while tracked flippers are used to overcome obstacles.

stair pitch angle. By using an IMU to provide orientation, our approach employs a state-feedback control law to improve the transitions between floor and stairs, ensuring smooth climbing and landing without collisions.

Unlike methods that depend on hard-to-obtain or estimate data, such as the precise contact point between the tracks and the ground, our strategy remains lightweight and practical. The robot differential kinematics is analyzed by treating it as an open-chain robotic manipulator constrained to move on the stair plane. Utilizing constrained manipulator theory, we design a control law supported by stability and convergence proof, offering a reliable solution for AATV navigation in stair environments

II. FLIPPERS CLOSED-LOOP CONTROL

Consider the lateral view of an AATV in Figure 2, with a main locomotion system, and equipped with two pairs of tracked flippers at the front and the rear, over a regular floor. The flippers are tied to the body frame by revolute joints. Let $\{0\}$ denote a fixed coordinate frame, $\{i\}$ with $i = 1,\ldots,4$ coordinate frames attached to the flippers, and $\{r\}$ a coordinate frame attached to the body centroid. Red arrows denote $\vec{x}$ direction for these frames, and blue arrows denote $\vec{z}$ direction. Let h_2 and h_3 be the respective heights of coordinate frames $\{2\}$ and $\{3\}$ with respect to the closer planes.

From Figure 2, one might note that the only necessary condition for a flipper track to fit the floor directly below is that two points on that track must be in contact with the floor. Accordingly, when the flipper tips touch the ground, the adjustment of the tracks can be formulated as a regulation problem: driving h_2 and h_3 to a reference height h_{ref} by controlling the joint velocities $\dot{\theta}_2$ and $\dot{\theta}_3$, respectively.

From Figure 2, one can consider the open chain robotic manipulator with a constraint presented in Figure 3. According to Gruebler's formula [12], the mechanism has $F = 3$ effective DoF

$$F = 3(N - g) + \sum_{i=1}^{g} f_i = 3, \tag{1}$$

where $N = 3$ is the number of links, $g = 4$ the number of joints and f_i is the number of DoF of joint i, with $f_i = \{2, 1, 2, 1\}$. An adequate approach for constrained manipulators with some effective DoF such that the active joints' Jacobian matrix is invertible is to rewrite passive joints as a linear combination of the active ones [12].

As such, let us then formulate the problem as follows: for a robot such as in Figure 2, it is desired a control strategy that automatically manages the flippers during the stair climbing, given that the only known variables are (1) robot orientation, (2) joints angular positions, and (3) stair pitch.

The proposed method divides the process of trespassing a stair into two phases. The first one is referred to as the transition on the bottom floor. It is defined at all moments when the robot is on the verge of touching or in touch with the floor and plane, which is defined by the stair step's edges. The other phase is referred to as the transition on the upper floor. Similarly, it is defined when the robot is on the verge of touching or in touch with the place defined as the stair steps' edges and the upper floor. In the following sections, we present the differential kinematic analysis and then use the performed analysis to model each one of the transition phases. Once the phases are modeled, we present a general control law with experimental results and final considerations.

A. Differential kinematics

Although exemplified in an ideal situation, one might note that during the transition between any two planes, the robot in Figure 2 can be generically interpreted as the kinematic serial chain of Figure 3. The first joint has two DoF once it actively advances with known constant forward speed v

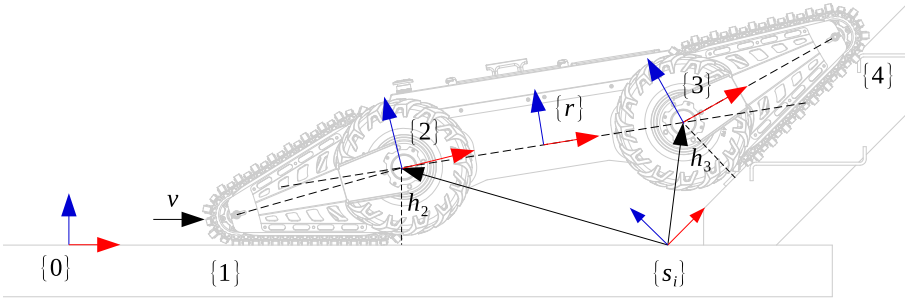

Fig. 2: Scheme of the front and rear flippers positioned such that their respective tracks fit the planes directly below. In the Figure, the robot is depicted in an ideal position, right as it should be, during the transition on the bottom floor.

and passively rotates with velocity $\dot{\theta}_1$. The second and third revolute joints are active, rotating with velocities $\dot{\theta}_2$ and $\dot{\theta}_3$ respectively. The last joint has another two DoFs, moving in the plane's x_{s_i} direction and rotating with velocity $\dot{\theta}_4$. As one might notice, the number of actuated joints allows us to leave for the operator the decision to advance at a given velocity, as the flippers' management control does the work of positioning the flippers.

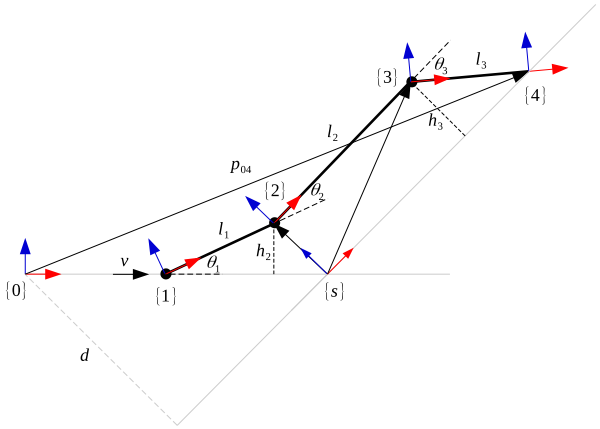

Fig. 3: Frames $\{1\}$ and $\{4\}$ in contact with different planes. Here, h_2 and h_3 are computed along z_0 and z_s, and the robot advances aligned with x_0.

Consider the kinematic chain in Figure 3 with flippers supported in two generic planes. Let z_2 and z_3 denote vectors normal to the surfaces directly below the respective joints and x_{a_1} be the direction of advance for frame 1. Also, let p_{ij} denote the position of j relative to i. Note that frame 4 is subject to a constraint given by

$$z_3^T\, p_{04} - d = 0, \tag{2}$$

where

$$p_{04} = p_{01} + l_1\, R_{01}\, \vec{x} + l_2\, R_{02}\, \vec{x} + l_3\, R_{03}\, \vec{x}. \tag{3}$$

The time derivative of (2) is given by

$$z_3^T\, \dot{p}_{04} = 0 \tag{4}$$

where

$$\begin{aligned} \dot{p}_{04} = \dot{p}_{01} + \hat{y}\, p_{12}\, \dot{\theta}_1 + \hat{y}\, p_{23}\, (\dot{\theta}_1 + \dot{\theta}_2) \\ + \hat{y}\, p_{34}\, (\dot{\theta}_1 + \dot{\theta}_2 + \dot{\theta}_3) \end{aligned} \tag{5}$$

with $\hat{y}$ being a skew-symmetric matrix defined as $\hat{y} = y\times$. Since

$$\dot{p}_{01} = v\, x_{a_1}, \tag{6}$$

by substituting (5) and (6) in (4), it is possible to write

$$\begin{aligned} z_3^T \big(v\, x_{a_1} + \hat{y}\, p_{12}\, \dot{\theta}_1 + \hat{y}\, p_{23}\, (\dot{\theta}_1 + \dot{\theta}_2) \\ + \hat{y} p_{34}\, (\dot{\theta}_1 + \dot{\theta}_2 + \dot{\theta}_3)\big) = 0. \end{aligned} \tag{7}$$

Let us separate the active joints and the passive ones as

$$\dot{\theta}_p = \dot{\theta}_1, \tag{8}$$

$$\dot{\theta}_a = \begin{bmatrix} \dot{\theta}_2 & \dot{\theta}_3 \end{bmatrix}^T. \tag{9}$$

Then, equation (7) can be rewritten as

$$\begin{aligned} z_3^T \big(v\, x_{a_1} + \hat{y}\, \left(p_{12} + p_{23} + p_{34}\right)\, \dot{\theta}_p \\ + \hat{y}\, \begin{bmatrix} p_{23} + p_{34} & p_{34} \end{bmatrix}\, \dot{\theta}_a\big) = 0 \end{aligned} \tag{10}$$

and manipulated to conclude that

$$\dot{\theta}_p = -\frac{z_3^T}{z_3^T\, J_p} \left(v\, x_{a_1} + J_a\, \dot{\theta}_a\right), \tag{11}$$

where $J_p \in \mathbb{R}^{3\times 1}$ is

$$J_p = \hat{y}\, \left(p_{12} + p_{23} + p_{34}\right), \tag{12}$$

and $J_a \in \mathbb{R}^{3\times 2}$ is

$$J_a = \hat{y}\, \begin{bmatrix} p_{23} + p_{34} & p_{34} \end{bmatrix}. \tag{13}$$

B. Height kinematic model

As previously presented, the strategy proposed in this paper consists of regulating joints 2 and 3 heights with respect to the plane directly below. In Figure 3 let h_2 be defined as

$$h_2 = z_2^T (p_{02} - p_{0s}), \tag{14}$$

and it's according time derivative

$$\dot{h}_2 = z_2^T\, \dot{p}_{02}. \tag{15}$$

Since

$$\dot{p}_{02} = v\, x_{a_1} + \hat{y}\, p_{12}\, \dot{\theta}_1, \tag{16}$$

by substituting (8) and (11) in (16), and the result in (15), it is possible to write $\dot{h}_2$ as function of active joints speed $\dot{\theta}_a$

$$\dot{h}_2 = -z_2^T\, \hat{y}\, p_{12}\, \frac{z_3^T}{z_3^T J_p} \left(v\, x_{a_1} + J_a\, \dot{\theta}_a \right). \tag{17}$$

Similarly, to do the same for h_3, define

$$h_3 = z_2^T (p_{03} - p_{0s}) \tag{18}$$

and its time derivative

$$\dot{h}_3 = z_3^T \dot{p}_{03}, \tag{19}$$

where

$$\dot{p}_{03} = v\, x_{a_1} + \hat{y}\, p_{12}\, \dot{\theta}_1 + \hat{y}\, p_{23}\, \left(\dot{\theta}_1 + \dot{\theta}_2 \right). \tag{20}$$

Substituting (8) and (11) in (20), and the result in (19), it follows

$$\begin{aligned} \dot{h}_3 = z_3^T \Bigg(& v\, x_{a_1} - \hat{y}\, \left(p_{12} + p_{23} \right) \frac{z_3^T}{z_3^T J_p} \left(v\, x_{a_1} + J_a\, \dot{\theta}_a \right) \\ & + \hat{y}\, \begin{bmatrix} p_{23} & 0_{3\times 1} \end{bmatrix} \dot{\theta}_a \Bigg). \end{aligned} \tag{21}$$

At this time, it should be clear to the reader that equations (17) and (21) are velocities of the respective coordinate frames. After some manipulations, we can split terms related to the forward speed advance v from those relative to the rotating speed of active joints $\dot{\theta}_a$. Therefore, the referred equation (17) can be written as

$$\dot{h}_2 = v_2 + J_2^T\, \dot{\theta}_a\,, \tag{22}$$

with

$$v_2 = -v\, z_2^T\, \hat{y}\, p_{12}\, \frac{z_3^T}{z_3^T J_p}\, x_{a_1}\,, \tag{23}$$

$$J_2^T = -z_2^T\, \hat{y}\, p_{12}\, \frac{z_3^T}{z_3^T J_p}\, J_a\,. \tag{24}$$

and equation (21) as

$$\dot{h}_3 = v_3 + J_3^T\, \dot{\theta}_a\,, \tag{25}$$

with

$$v_3 = v\, z_3^T \left(I_{3\times 3} - \hat{y}\, \left(p_{12} + p_{23} \right) \frac{z_3^T}{z_3^T J_p} \right) x_{a_1}\,, \tag{26}$$

$$J_3^T = z_3^T\, \hat{y} \left(\begin{bmatrix} p_{23} & 0_{3\times 1} \end{bmatrix} - \left(p_{12} + p_{23} \right) \frac{z_3^T}{z_3^T J_p}\, J_a \right). \tag{27}$$

Note, then, that for all AATVs such as the ones presented here, while moving with flippers supported by whatever two planes with defined normal vectors, the system can be written down in a linear form as

$$\dot{h} = \nu(\theta, v) + J(\theta)\, \dot{\theta}_a\,, \tag{28}$$

where

$$h = \begin{bmatrix} h_2 & h_3 \end{bmatrix}^T, \tag{29}$$

$$\nu(\theta, v) = \begin{bmatrix} v_2 & v_3 \end{bmatrix}^T, \tag{30}$$

and

$$J(\theta) = \begin{bmatrix} J_2^T \\ J_3^T \end{bmatrix}. \tag{31}$$

C. Flippers management control law

Consider the system (28). Let $h_r \in \mathbb{R}^2$ be a constant height reference. Let e be the error defined as

$$e = h - h_r \tag{32}$$

and its time derivative

$$\dot{e} = \dot{h}\,.$$

Therefore

$$\dot{e} = \nu + J(\theta)\, \dot{\theta}_a. \tag{33}$$

It is desired a closed-loop state feedback control law such that the origin of the system (33) is asymptotically stable under the following assumptions: (**A1**) the active joints speed vector is the control input, i.e. $\dot{\theta}_a = u$; (**A2**) the term $\nu(\theta, v)$ is limited and known; (**A3**) $J(\theta)$ is a full rank matrix.

The following equation presents the proposed control law

$$u = -J^{-1}(\theta) \left(\nu + k_p\, e + k_i \int_0^t e(\tau)\, d\tau \right), \tag{34}$$

where k_p, $k_i \in \mathbb{R}^{2\times 2}$ are constant positive definite matrices.

Consider system (33), the control law (34), and assumptions (**A1-A3**). In a closed-loop, the integral term provides the second-order dynamics

$$\ddot{e} + k_p\, \dot{e} + k_i\, e = 0\,. \tag{35}$$

Thus, the equilibrium point $(e, \dot{e}) = 0$ is globally exponentially stable and the linear error dynamic (35) is globally exponentially stable.

D. State machine for transitions

During transitions, the primary objective of the robot's flippers is to induce the entire body to move toward a desired surface. While in an active state, the control algorithm autonomously regulates the flippers to a height reference h_{ref} equal to the wheel's radius, ensuring alignment of the robot's tracks with their respective surfaces. In the defined transitions, the state-feedback law (34) relies on determining height measurements h_2 and h_3. These heights are computed based on the normal vectors of the planes directly beneath the coordinate frames $\{2\}$ and $\{3\}$ origins. Additionally, the direction of motion of frame 1 varies depending on the particular transition being executed. Although the Cartesian position was used for process modeling, direct position measurements are not requisite once certain variables are available: the robot's pitch angle θ_r from an IMU, the angular positions of joints θ_2 and θ_3 from encoders, and the stair pitch θ_s. To effectively manage the provision of essential heights and directions required for the control law, a finite state machine is employed to determine the appropriate approach for calculating heights, the Jacobian matrix, and the velocity component.

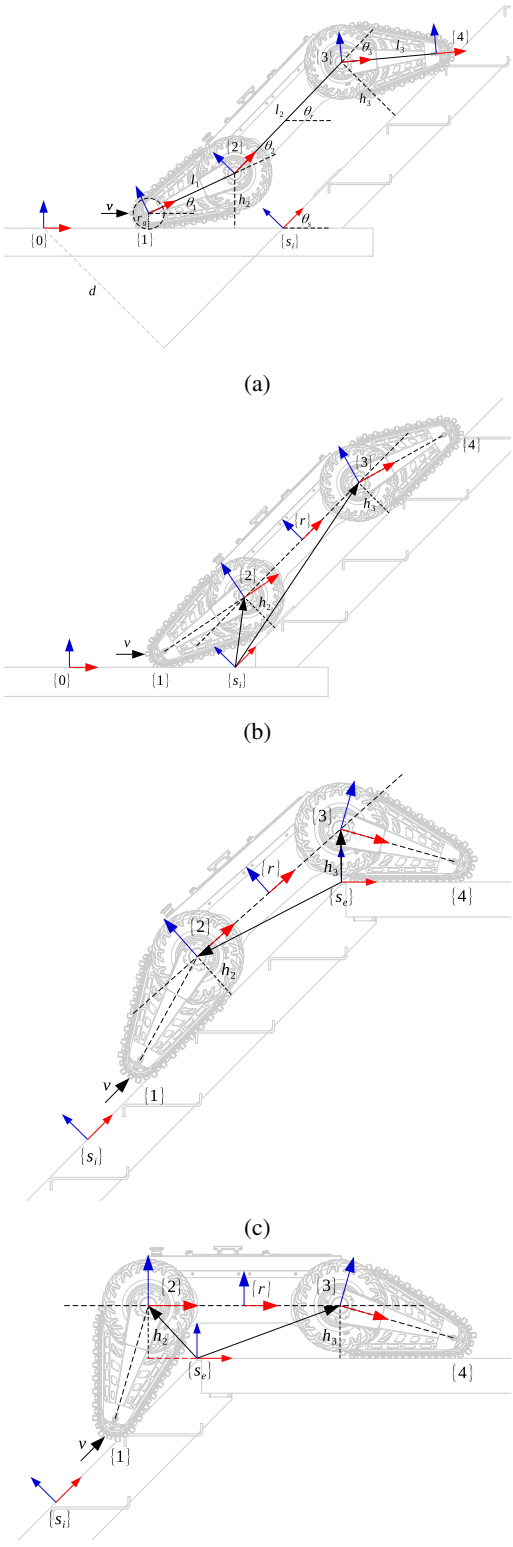

Fig. 4: Transition diagrams illustrating the management of height calculation during floor transitions and the robot's configurations for different transition stages.

Before introducing the state machines, in Figure 4a, it is prudent to define r_g as the radius of a gear located at the end of an arm, a parameter of importance for height measurements. Note that the joint position of the first joint remains known throughout the process. Illustrated in Figure 4c, the robot's configuration reveals the possibility to calculate h_2 and h_3 by following the kinematic chain, considering known values of θ_r, θ_s, and r_g.

The finite state machine in Figure 6 governs height calculations during floor transitions. The robot's kinematic chain defines movement variables: $\theta_1 = \theta_r - \theta_2$ and $\theta_4 = \theta_1 + \theta_2 + \theta_3 \pm \theta_s$ for inferior and upper floors, respectively.

The robot starts at 0_{inf} on the bottom floor, aligned with the stairs. It progresses to A_{inf} upon operator command. Closed-loop control engages in A_{inf} (Figure 4a, where the robot is presented in a non-ideal position), transitioning autonomously to B_{inf} when the robot's pitch aligns with the stairs or to state 0 when it matches the floor's pitch. In B_{inf} (Figure 4b), the rear tracks stay in contact with the floor. As it progresses, both flippers move automatically to match the stairs' inclination, smoothing out the transition step for either possible states Nav or back to A_{inf}.

The robot aligns with the stairs in the Nav state for the upper floor transition. It advances to A_{sup} upon operator command (Figure 4c). Closed-loop control in A_{sup} progresses autonomously to B_{sup} when the robot's pitch aligns with the upper floor or to Nav when it matches the stair's pitch. In B_{sup} (Figure 4d), the rear flippers gradually elevate for a smooth landing, and the state machine can transition to 0_{sup} once a minimal safety distance is reached.

Remark 1: To avoid hull collision while traversing from the stairs to the upper floor (Figure 5), the regulated heights must respect the condition

$$h_2 > \left(l_2 - \frac{h_3'}{\sin(\theta_r)}\right)\sin(\theta_s - \theta_r) + \frac{d_h}{\cos(\theta_s - \theta_r)}, \qquad (36)$$

where d_h is the distance from the hull's bottom to the robot's center-line, l_2 the distance between $\{2\}$ and $\{3\}$, and

$$h_3' = h_3 - \frac{d_h}{\cos(\theta_r)}.$$

■

Various navigation strategies are available to ensure that the robot remains centered and avoids stair borders, enabling seamless navigation on stairs. They range from simple proportional controllers to more complex methodologies.

III. EXPERIMENTAL RESULTS

To evaluate the proposed method for flipper management during stair-climbing tasks, the AATV Rosi [3] is used. The robot's primary locomotion system is the wheels driven by independent motors coupled with high-reduction gearboxes. The motion control software runs on an embedded PC/104 with an Intel Core i7 processor and was developed using the ROS framework. An Advanced Navigation Motus IMU and an Intel Realsense D435 RGB-D camera were used for orientation sensing and environment perception, respectively. Custom ROS packages were developed for stair detection and

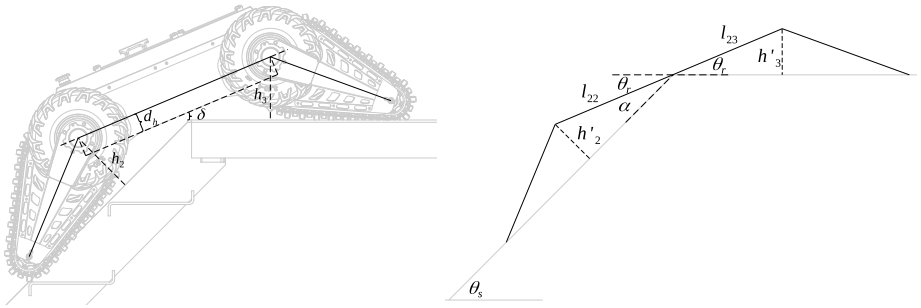

Fig. 5: The clearance $\delta = 0$ signals a collision of the hull and the step edge. The schematic on the right defines the trigonometric relationship required to maintain $\delta > 0$ for collision avoidance.

climbing. The algorithm is deployed on the robot's embedded PC, and the robot is commanded to climb two stairs.

This section presents the results for ascending two stairs. Descending is also tested, but the results are omitted for conciseness, as the methodology and observations were similar to the ascent. Stair detection and modeling followed the 3D normal-based edge detection method described in [13].

Each of the results presented further in the text comprises two figures. The first (Figures 8, 10, 12 and 14) with the sequence of maneuvers performed by the robot during the ascending process, and the second (Figures 9, 11, 13 and 15) with the height error, control input, and robot pitch compared with that of the stair.

A. *First Experiment*

The first experiment utilizes the staircase shown in Figure 7, featuring treads and risers of 300 mm and 170 mm, respectively, and a pitch of approximately 30°. The initial setup for the experiment is presented in Figure 8. The robot is positioned on its wheels with flippers raised, aligned to the stair steps, and placed at an appropriate distance. A command to advance at a constant speed of $v = 0.1$ m/s is issued, with flippers controlled autonomously as illustrated in the image sequence.

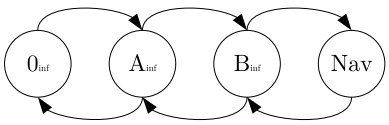

(a) Bottom floor transition

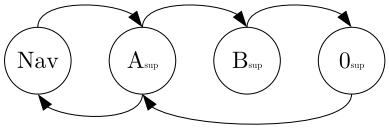

(b) Upper floor transition

Fig. 6: State machines for managing height calculation during floor transitions.

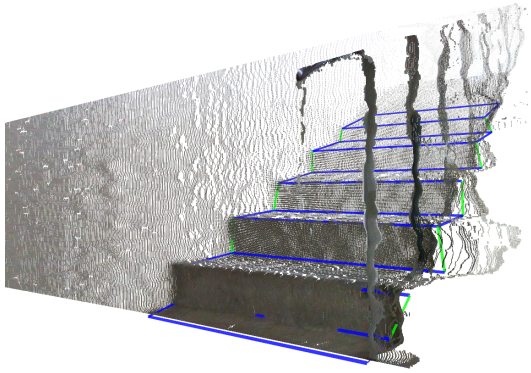

Fig. 7: Staircase used in the first experiment. The blue lines surround the treads, while the green lines connect the limits between consecutive treads to form the risers.

1) Transition to Stair: The sequence of images in Figure 8 illustrates the robot transitioning from the bottom floor to the stair plane. Initially, the flippers are away from the desired configuration, causing an initial saturation at the beginning. The height error shows an underdamped response with no steady-state error. The disturbance observed towards the end is due to the state transition, which changes the method for calculating the second joint's height. The pitch error highlights the strategy's ability to make the robot's orientation match the stairs while climbing.

2) Transition to Upper Floor: The same procedure is repeated for the superior transition. As the robot approaches the edge of the last step with slightly elevated flippers, the command to advance is issued again. In Figure 11, initially, since the front flippers are off the ground, for a brief moment, they do not affect the robot's pitch, causing a mismatch between calculated and actual heights. This caused the rear arm errors to respond distinctively in the first seconds. Finally, the pitch error during this transition demonstrates how the strategy manages the robot's orientation to smoothly match the upper floor.

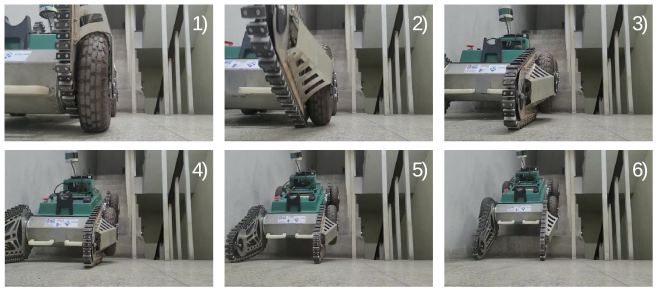

Fig. 8: Sequence of images showing the transition to the stair plane, starting at the bottom floor (image 1) and ending when Rosi completes the transition to the stair plane (image 6).

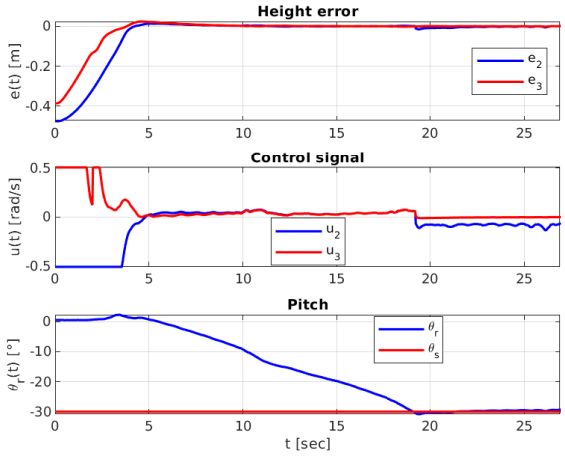

Fig. 9: Height error during the transition from the bottom floor to the stair plane.

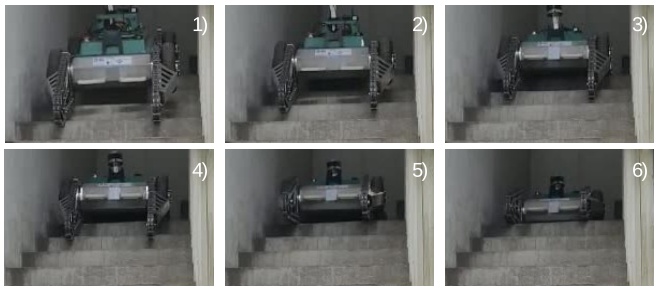

Fig. 10: Sequence of images during the superior transition.

B. Second Experiment

Here a more challenging staircase is tested. This staircase features treads and risers measuring 230 mm and 180 mm, respectively, and has a pitch of approximately 38°. Additionally, the edges of the steps have smoother surfaces and a greater radius of curvature, impairing traction and making it more difficult than the first staircase. Due to its greater length (4.1 meters) and lateral visualization, this ladder allows a better understanding of the maneuvers performed by the arms.

1) Transition to Stair: The sequence of images in Figure 12 presents the robot transitioning from the bottom floor to the stair plane. As in the first step, the transition includes a noticeable height error jump of around 35 seconds due to the state machine logic used.

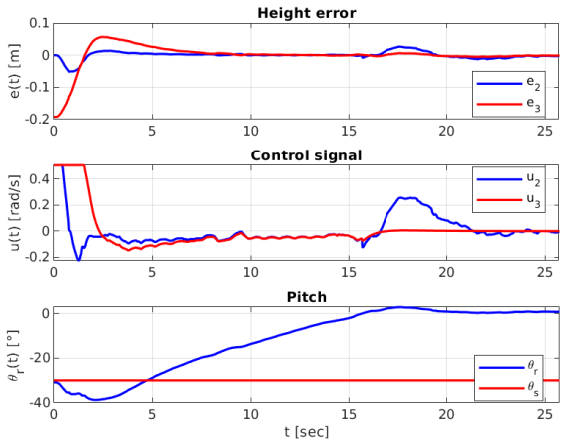

Fig. 11: Height error during the transition from the stair plane to the upper floor.

Fig. 12: Sequence of images in the transition to the stair plane, starting at the bottom floor (image 1) and ending when Rosi completes the transition to the stair plane (image 6).

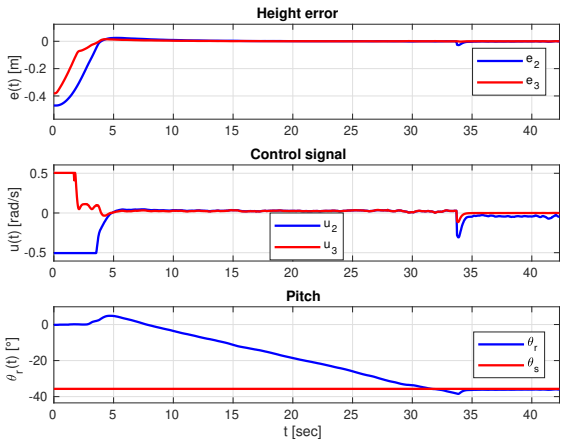

Fig. 13: Height error during the transition from the bottom floor to the stair plane.

2) Transition to Upper Floor: The sequence of images in Figure 14 shows the robot transitioning from the stair plane to the upper floor. Initial discrepancies between calculated and actual heights are due to the front flippers being momentarily off the ground, leading to distinct initial errors in the rear arms. The control strategy effectively manages these discrepancies, stabilizing the robot's pitch and ensuring a smooth transition to the upper floor, as shown in Figure 15. The sudden stop around 20 seconds is due to the impossibility of advancing further because of a wall, without compromising the results of the experiment.

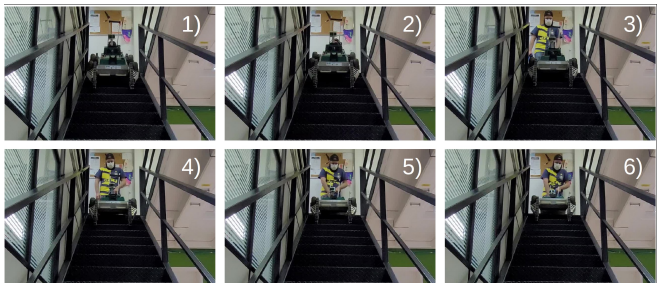

Fig. 14: Sequence of images in the transition from the stair plane to the upper floor, starting on the stair plane (image 1) and ending when Rosi completes the transition to the upper floor (image 6).

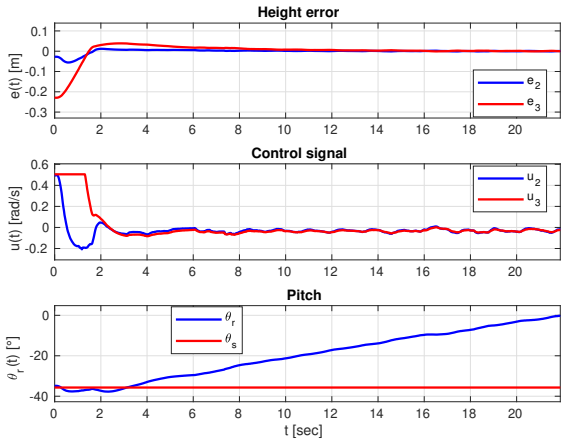

Fig. 15: Height error during the transition from the stair plane to the upper floor.

IV. CONCLUSION

This paper presents a novel approach to model an AATV while moving on a set of stairs. A state-feedback control law for flippers management was provided with stability and convergence analysis. The experimental results validate both the proposed modeling and control strategy. The robot can continuously best-fit flippers to surfaces during transitions, while other algorithms can control other variables, such as heading.

The proposed methodology is effective in managing flippers during stair transposal, as evidenced by the height and pitch error. The calculation of heights and projection directions in the control law depends on the states of a state machine, and as such, small disturbances are expected in transition events. However, its effects are minimal and do not compromise the robot's ability to traverse stairs. The integral term maintained flippers in their corresponding surfaces, besides the constant advance, track slippage, and missed support points.

While this paper provides a solid foundation for the task, future work will focus on expanding its validation through additional experimental results across diverse scenarios and other obstacles. We also intend to conduct comprehensive benchmarks against other state-of-the-art methods, such as reinforcement learning-based approaches. These extensions, which would exceed the scope and space constraints of the current paper, will further solidify the robustness of the proposed methodology.

REFERENCES

[1] L. Bruzzone and G. Quaglia, "Review article: locomotion systems for ground mobile robots in unstructured environments," *Mechanical Sciences*, vol. 3, pp. 49–62, 07 2012.

[2] M. Hutter, C. Gehring, A. Lauber, F. Gunther, C. D. Bellicoso, V. Tsounis, P. Fankhauser, R. Diethelm, S. Bachmann, M. Blösch, *et al.*, "Anymal-toward legged robots for harsh environments," *Advanced Robotics*, vol. 31, no. 17, pp. 918–931, 2017.

[3] F. Rocha, G. Garcia, R. Pereira, H. Faria, and et. al, "Rosi: A robotic system for harsh outdoor industrial inspection - system design and applications," *Journal of Intelligent & Robotic Systems*, vol. 103, 10 2021.

[4] M. Gianni, F. Ferri, M. Menna, and F. Pirri, "Adaptive robust three-dimensional trajectory tracking for actively articulated tracked vehicles," *Journal of Field Robotics*, vol. 33, no. 7, pp. 901–930, 2016.

[5] M. Hinderer, P. Friedrich, and B. Wolf, "An autonomous stair-climbing wheelchair," *Robotics and Autonomous Systems*, vol. 94, pp. 219–225, 2017.

[6] İrem Mertyüz, A. K. T. ldızı, B. Taşar, A. B. Tatar, and O. Yakut, "Fuhar: A transformable wheel-legged hybrid mobile robot," *Robotics and Autonomous Systems*, vol. 133, p. 103627, 2020.

[7] S. Steplight, G. Egnal, S.-H. Jung, D. B. Walker, C. J. Taylor, and J. P. Ostrowski, "A mode-based sensor fusion approach to robotic stair-climbing," in *IEEE/RSJ Int. Conf. on Intelligent Robots and Systems (IROS)*, vol. 2, 2000, pp. 1113–1118.

[8] A. I. Mourikis, N. Trawny, S. I. Roumeliotis, D. M. Helmick, and L. Matthies, "Autonomous stair climbing for tracked vehicles," *The Int. Journal of Robotics Research*, vol. 26, no. 7, pp. 737–758, 2007.

[9] E. Mihankhah, A. Kalantari, E. Aboosaeedan, H. D. Taghirad, S. Ali, and A. Moosavian, "Autonomous staircase detection and stair climbing for a tracked mobile robot using fuzzy controller," in *IEEE Int. Conf. on Robotics and Biomimetics*, 2009, pp. 1980–1985.

[10] Y. Okada, K. Nagatani, K. Yoshida, S. Tadokoro, T. Yoshida, and E. Koyanagi, "Shared autonomy system for tracked vehicles on rough terrain based on continuous three-dimensional terrain scanning," *Journal of Field Robotics*, vol. 28, no. 6, pp. 875–893, 2011.

[11] D. Endo, A. Watanabe, and K. Nagatani, "Stair climbing control of 4-degrees-of-freedom tracked vehicle based on internal sensors," in *IEEE Int. Symposium on Safety, Security, and Rescue Robotics*, 2016, pp. 112–117.

[12] K. M. Lynch and F. C. Park, *Modern Robotics: Mechanics, Planning, and Control*, 1st ed. USA: Cambridge University Press, 2017.

[13] H. Harms, E. Rehder, T. Schwarze, and M. Lauer, "Detection of ascending stairs using stereo vision," *IEEE/RSJ Int. Conf. on Intelligent Robots and Systems (IROS)*, pp. 2496–2502, 2015.